Hidden Structural Features of Multicompartment Micelles Revealed by Cryogenic Transmission Electron Tomography

Tina I. Löbling,[†,⊥] Johannes S. Haataja,[‡,⊥] Christopher V. Synatschke,[†] Felix H. Schacher,[§] Melanie Müller,[†] Andreas Hanisch,[†] André H. Gröschel,[*,‡] and Axel H. E. Müller[*,†,∥]

[†]Makromolekulare Chemie II, Universität Bayreuth, D-95440 Bayreuth, Germany, [‡]Department of Applied Physics, School of Science, Aalto University, FIN-02150 Espoo, Finland, [§]Institut für Organische Chemie und Makromolekulare Chemie and Jena Center for Soft Matter (JCSM), Friedrich-Schiller-Universität Jena, D-07743 Jena, Germany, and [∥]Institut für Organische Chemie, Johannes Gutenberg-Universität Mainz, D-55099 Mainz, Germany. [⊥]T. I. Löbling and J. S. Haataja contributed equally to this work.

ABSTRACT The demand for ever more complex nanostructures in materials and soft matter nanoscience also requires sophisticated characterization tools for reliable visualization and interpretation of internal morphological features. Here, we address both aspects and present synthetic concepts for the compartmentalization of nanoparticle peripheries as well as their *in situ* tomographic characterization. We first form negatively charged spherical multicompartment micelles from ampholytic triblock terpolymers in aqueous media, followed by interpolyelectrolyte complex (IPEC) formation of the anionic corona with bis-hydrophilic cationic/neutral diblock copolymers. At a 1:1 stoichiometric ratio of anionic and cationic charges, the so-formed IPECs are charge neutral and thus phase separate from solution (water). The high chain density of the ionic grafts provides steric stabilization through the neutral PEO corona of the grafted diblock copolymer and suppresses collapse of the IPEC; instead, the dense grafting results in defined nanodomains oriented perpendicular to the micellar core. We analyze the 3D arrangements of the complex and purely organic compartments, *in situ*, by means of cryogenic transmission electron microscopy (cryo-TEM) and tomography (cryo-ET). We study the effect of block lengths of the cationic and nonionic block on IPEC morphology, and while 2D cryo-TEM projections suggest similar morphologies, cryo-ET and computational 3D reconstruction reveal otherwise hidden structural features, *e.g.*, planar IPEC brushes emanating from the micellar core.

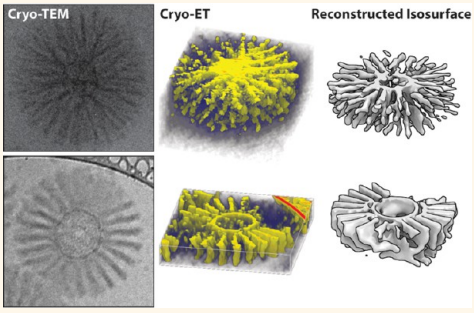

KEYWORDS: cryo-electron tomography · interpolyelectrolyte complexes · multicompartment micelles · nanoparticles · self-assembly

The synthetic design of complex colloidal particles underwent great progress in the nanoengineering of particle shape (anisotropy), compartmentalization (core or surface patches), and functionality (directional forces).[1−3] While top-down procedures dominate particle structuring on the micrometer scale, bottom-up concepts continue to evolve as potential preparative tools on the nanoscale.[4−6] In this regard, the self-assembly of block copolymers offers straightforward strategies to unify multiple environments within one nanoobject.[7] The number of compartments is proportional to the number of incompatible polymer blocks, where ABC triblock terpolymers already display a rich repertoire of bulk and solution morphologies.[8,9] Amphiphilic block copolymers are a highly frequented source for water-stable polymeric particles, as they spontaneously self-assemble into a hydrophobic core stabilized by either a nonionic (*e.g.*, poly(ethylene oxide), PEO) or a polyionic hydrophilic corona.[10−12] A charged corona opens up further coordination possibilities, *e.g.*, for templating, nanoparticle immobilization (inorganic or biological), or complementarily charged polyelectrolytes. Ballauff *et al.* immobilized anionic metal nanoparticles in

* Address correspondence to andre.groschel@aalto.fi; axel.mueller@uni-mainz.de.

Received for review July 29, 2014 and accepted September 7, 2014.

Published online September 07, 2014
10.1021/nn504197y

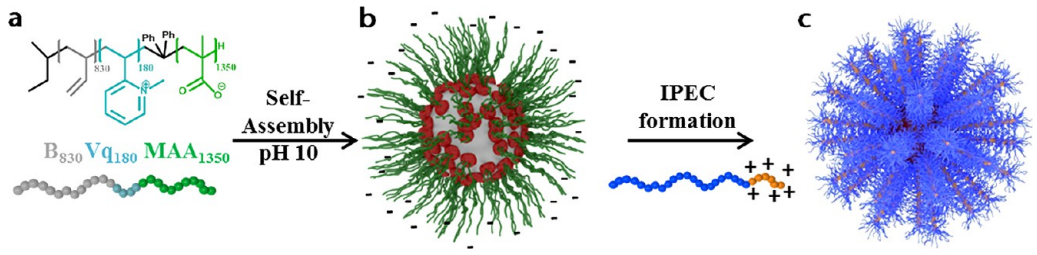

Scheme 1. (a) Chemical Structure of the $B_{830}Vq_{180}MAA_{1350}$ triblock terpolymer. (b) Schematic of the BVqMAA multicompartment micelles with PB core (gray), PVq/PMAA *im*-IPEC patches (red), and excess PMAA corona (green) in aqueous solution. (c) Complexation of PMAA with bis-hydrophilic cationic diblock copolymers to form particles with anisotropic IPEC domains.

cationic spherical polyelectrolyte brushes, creating hybrid heterogenic catalyst systems.[13] Proteins or enzymes were also captured by either cationic or anionic brushes.[14−17] To compartmentalize the polyionic corona brush, polymer blending[4] and intra- or interpolyelectrolyte complex (IPEC) formation have proven their efficiency.[18−23] Ionic polymers coassemble with complementarily charged blocks through noncovalent electrostatic interactions to form a new compartment with high incompatibility to the surrounding phases (polymer blocks, water, or interfaces).[24−26] Applying this concept, vesicles with IPEC walls were coassembled from two block ionomers in organic solvents[27] as well as in water,[28,29] Janus particles with IPEC cores in water,[30] and vesicles with nanosegregated walls *via* salt-induced chelation.[31]

In previous works we demonstrated that polybutadiene-*block*-poly(1-methyl-2-vinylpyridinium)-*block*-poly(methacrylic acid) (PB-*b*-PVq-*b*-PMAA, BVqMAA) triblock terpolymers self-assemble into multicompartment micelles with a soft PB core, intramicellar IPEC (*im*-IPEC) patches of PVq/PMAA, and a short stabilizing PMAA corona (~360 residual units of MAA).[20] Complexation of polycations with comparable length to the residual anionic corona usually led to homogeneous second IPEC shells.[21,22] In the case of a much longer anionic PMAA corona (~1170 residual units of MAA), IPECs with cationic homopolymers collapsed as irregularly shaped, discontinuous compartments onto the micellar core.[23] This segregation phenomenon led us to the hypothesis that the combination of a long PMAA corona and a bis-hydrophilic block copolymer with short polycationic blocks could generally phase-separate into a variety of anisotropic corona morphologies (Scheme 1).[32,33] Concepts to structure nanoparticle peripheries are desirable, because corona compartments are directly accessible for loading and modification, they allow (inter)particle recognition, and they provide directional forces for hierarchical self-assembly.[34−41]

Although research in many fields greatly benefits from higher structural complexity (*e.g.*, advanced gating materials, energy storage, nanoreactors, and biomedical applications), this also demands sophisticated methods to reliably characterize and visualize internal morphological features. In the case of entirely organic nanoparticles, transmission electron microscopy (TEM) usually is the first choice. This technique visualizes differences in electron contrast in the dried and often collapsed state. In the case of soft matter, particle flattening or buckling (*e.g.*, capsules) is a common drying artifact that has to be taken into account when discussing particle morphology. Cryogenic TEM (cryo-TEM) circumvents most of these issues through vitrification and *in situ* imaging of a thin solvent film that contains the specimen.[42] Although cryo-TEM is a valuable characterization tool in many scientific fields,[43] the obtained images are 2D projections of 3D objects. Overlapping internal features may complicate the analysis of complex nanostructures and may lead to false interpretations. Cryogenic transmission electron tomography (cryo-ET) on the other hand emerges as a powerful and versatile tool to obtain structural information in three dimensions.[44] Here, a series of 2D image projections is captured from the same vitrified particle (or area) at different viewing angles. After image alignment of the 2D images, a 3D tomogram can be reconstructed using computational methods. Although this technique is well established for biological matter characterization with nanometer resolution,[45] cryo-ET only gradually progresses to other research fields.[46−48] In particular, soft matter materials could benefit from *in situ* characterization, where particles become increasingly complex. Tomographic particle visualization is still challenging, because the contrast difference of (mostly) hydrocarbon constituents is usually low as compared to, for example, electron-dense inorganic nanoparticles, and long exposure times increase the risk of electron beam damage of particles or solvent film. So far, cryo-ET unfolds its full potential in aqueous solution, where contrast differences between solvent and hydrocarbon specimens are acceptable and vitrified films allow for sufficiently long exposure. It was only recently when Sommerdijk *et al.* used cryo-ET to resolve the structure of spherical polymer aggregates with an internally curved bicontinuous morphology self-assembled from amphiphilic double-comb diblock copolymers.[49] These and other works in the field of (cryogenic)

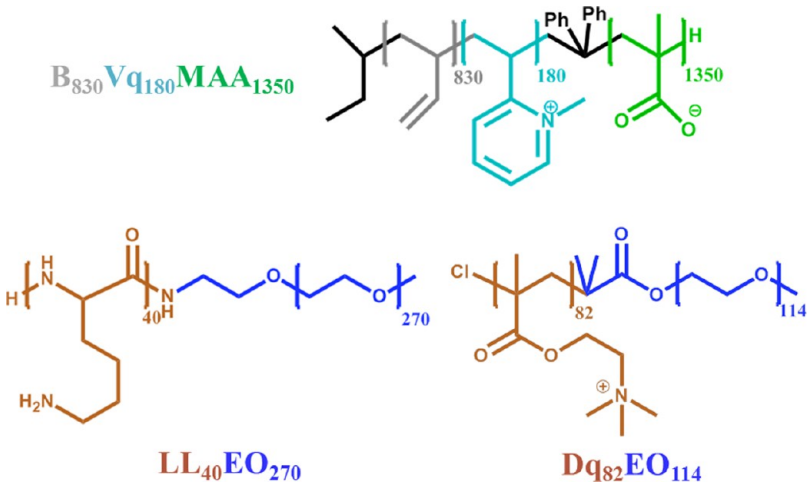

Chart 1. Chemical structures of the used triblock terpolymer and diblock copolymers.

tomography impressively demonstrated the benefits of 3D reconstruction for the interpretation of particle features toward a deeper understanding of the underlying formation mechanism.[50−54]

Here, we pursue two objectives, the structuring of compartmentalized organic nanoparticles as well as their in-depth tomographic characterization. We utilize ionic grafting of complementarily charged polyions to create ordered IPEC nanodomains within the charged corona of multicompartment micelles. A predefined mismatch in polyion chain length facilitates dense grafting of a predefined number of diblock copolymer chains per corona chain up to the point of charge neutralization. The large quantity of polymer chains and dense chain packing of the nonionic block causes massive overcrowding within the corona that suppresses collapse of the IPEC to globules, but instead forces corona chains to stretch into anisotropic IPEC morphologies. We then resolve the periodic 3D arrangements of the purely organic nanophases with cryogenic transmission electron tomography as an emerging *in situ* technique for soft matter characterization.

RESULTS AND DISCUSSION

Components for IPEC Formation. The triblock terpolymer $B_{830}Vq_{180}MAA_{1350}$ (subscripts denote the degree of polymerization; see Chart 1 and Table S1 of the Supporting Information) self-assembles into spherical multicompartment micelles in aqueous solution with an aggregation number of $N_{agg} \approx 650$ $B_{830}Vq_{180}MAA_{1350}$ chains per micelle (see the Supporting Information for calculations). As was shown earlier for a polymer with shorter PMAA block,[21] these $B_{830}Vq_{180}MAA_{1350}$ precursor micelles exhibit a hydrophobic PB core, intramicellar IPEC (*im*-IPEC) patches of PVq/PMAA on the surface, and an anionic corona of excess PMAA (Figure 1a). Dynamic light scattering (DLS) gives a hydrodynamic radius of $\langle R_h \rangle_{z,app}$ = 172 nm after *im*-IPEC formation (Figure S1) originating from the 1170 units of charged and noncoordinated MAA per corona chain. At pH ≥ 7 the MAA units are sufficiently deprotonated[20] (ζ-potential ≈ −32 mV) and are accessible for quantitative intermolecular complexation with cationic polymers (ζ-potential ≈ 0 mV).[21−23] For that, we use two bis-hydrophilic cationic diblock copolymers (Chart 1 and Table 1), poly(L-lysine)-*block*-poly(ethylene oxide) ($LL_{40}EO_{270}$) and quaternized poly(2-(dimethylamino)ethyl methacrylate)-*block*- poly(ethylene oxide) ($Dq_{82}EO_{114}$).

Both diblock copolymers, $LL_{40}EO_{270}$ and $Dq_{82}EO_{114}$, have comparable molecular weights and contain one cationic (PLL or PDq) and one nonionic water-soluble block (PEO). The block length of the polycation regulates the number of polymer chains that ionically graft per anionic PMAA corona chain, whereas the PEO block length determines the volume requirement of the grafted brush and acts as the new stabilizing corona. The differences in the length of both blocks should have distinct effects on chain packing and the resulting corona morphology. To calculate the mixing ratio of polyion chains, we define the charge ratio, $Z_{+/-}$, in eq 1. A value of $Z_{+/-} = 0$ corresponds to the PMAA corona without addition of polycations and $Z_{+/-} = 1$ to quantitative complexation with the polycationic block copolymers (charge neutralization).

$$Z_{+/-} = \frac{n_{\text{cationic}}}{n_{\text{anionic}}} = \frac{n_{\text{LL(orDq)}}}{n_{\text{MAA}} - n_{\text{Vq}}} \qquad (1)$$

In the following we will first give a detailed morphological characterization of IPECs formed by complexation of the $B_{830}Vq_{180}MAA_{1350}$ precursor micelles with $LL_{40}EO_{270}$ and $Dq_{82}EO_{114}$ and then discuss particle composition and chain arrangements.

Self-Assembly of IPEC1. Figure 1b shows the self-assembly strategy as well as the resulting nanostructure after IPEC formation of the $BVqMAA_{1170}$ precursor micelles with $LL_{40}EO_{270}$ (1170 units of MAA left after *im*-IPEC formation). At quantitative complexation of the micellar corona (ζ-potential ≈ −2 mV), we observe

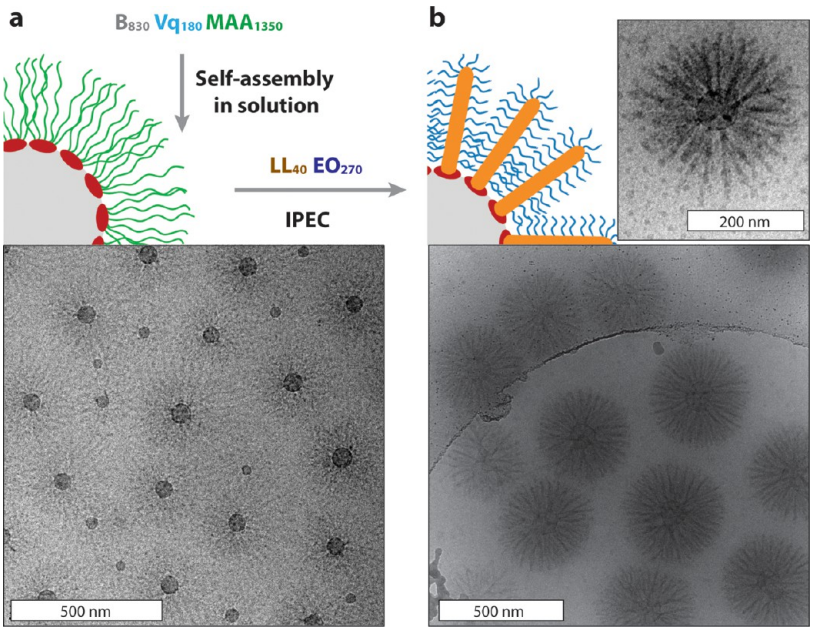

Figure 1. Formation of $BVqMAA_{1170}$ precursor micelles and IPEC1 ($BVqMAA_{1170}/LL_{40}EO_{270}$). (a) Solution self-assembly of $BVqMAA_{1170}$, cryo-TEM image, and schematic of the micelles with PB core (gray), PVq/PMAA *im*-IPEC patches (red), and excess PMAA corona (green) in pH 10 buffer solution. (b) Complexation of PLL (brown) with PMAA (green) in pH 7 buffer solution results in bottlebrush formation of IPEC1 (orange) stabilized by PEO brush (blue). The inset shows one of the IPEC1 micelles at higher magnification.

TABLE 1. Specification of Cationic Bis-Hydrophilic Diblock Copolymers

polymer	DP (polycation)	DP (PEO)	M_n [kg/mol][a]	PDI[b]
$LL_{40}EO_{270}$	40	270	17.7	1.05
$Dq_{82}EO_{114}$	82	114	17.9	1.17

[a] Calculated from ^{1}H NMR using the M_n of the PEO block provided by the supplier. [b] Determined with SEC in DMF (protected $LL_{40}EO_{270}$) or THF ($D_{82}EO_{114}$) as eluent and PEO standards.

an overall spherical shape with ray-like protrusions, the appearance of which is reminiscent of sea urchins. We reported about this IPEC morphology in a previous work, where we focused on the application of the highly PEGylated micelles as remarkably effective drug carrier systems in photodynamic cancer therapy.[32] Here, we subject this intricate morphology to a detailed structural characterization to determine its origin.

According to eq 1, 29.3 equiv of $LL_{40}EO_{270}$ is required to reach charge neutral conditions, $Z_{+/-} = 1$. Considering the $N_{agg} \approx 650$ of the $BVqMAA_{1170}$ precursor micelle, 650 PMAA chains in the corona of one micelle accommodate approximately 19 000 diblock copolymer chains. As illustrated in Figure 1b, the PMAA chains (green) undergo IPEC formation with the PLL block (brown) and most likely form a cylindrical brush (orange) stabilized by the PEO corona (blue). Two main parameters dominate the formation of an anisotropic IPEC: (i) the mismatch of chain lengths of polyionic blocks, PMAA and PLL, and (ii) the resulting overcrowding and dense packing of diblock copolymer chains within the confined space of the particle corona. To validate these observations and gain a deeper insight into the morphology, we further characterized these micellar IPECs by means of cryo-ET.

Cryo-ET Characterization of IPEC1. To extract more information on the architecture and to confirm the proposed cylindrical brush morphology of IPEC1, we performed cryo-ET, *i.e.*, a series of 2D cryo-TEM images of the same area at tilt angles from −69° to +69°, allowing 3D reconstruction after image alignment (Figure 2, see Methods and Supporting Movies, SM1 and SM2). For cryo-ET, a high electron acceleration voltage (here 300 kV) is beneficial to minimize beam damage to the sample and matrix. Yet, this poses challenges for visualizing soft matter, because less interaction of the electron beam with the organic material also reduces contrast. The soft nanoparticles proved surprisingly resilient against electron beam damage, and we recorded a total of 46 images in 3° increments (while observing noticeable degradation of the supporting carbon film in some cases). Figure 2a shows one particle measured with cryo-ET, and Figure 2b the calculated 3D reconstruction using the maximum entropy iterative method (see Methods and the Supporting Information). The isosurface model shows a compartmentalized corona structure, where single rays support the assumption of "sea urchin-like" morphology (Figure 2c). At first sight, the arrangement of the cylindrical IPECs seems chaotic, but from the side view we anticipate the onset of a hexagonal order (Figure 2d). Also the top view of the middle slice supports single IPEC rays protruding from the spherical

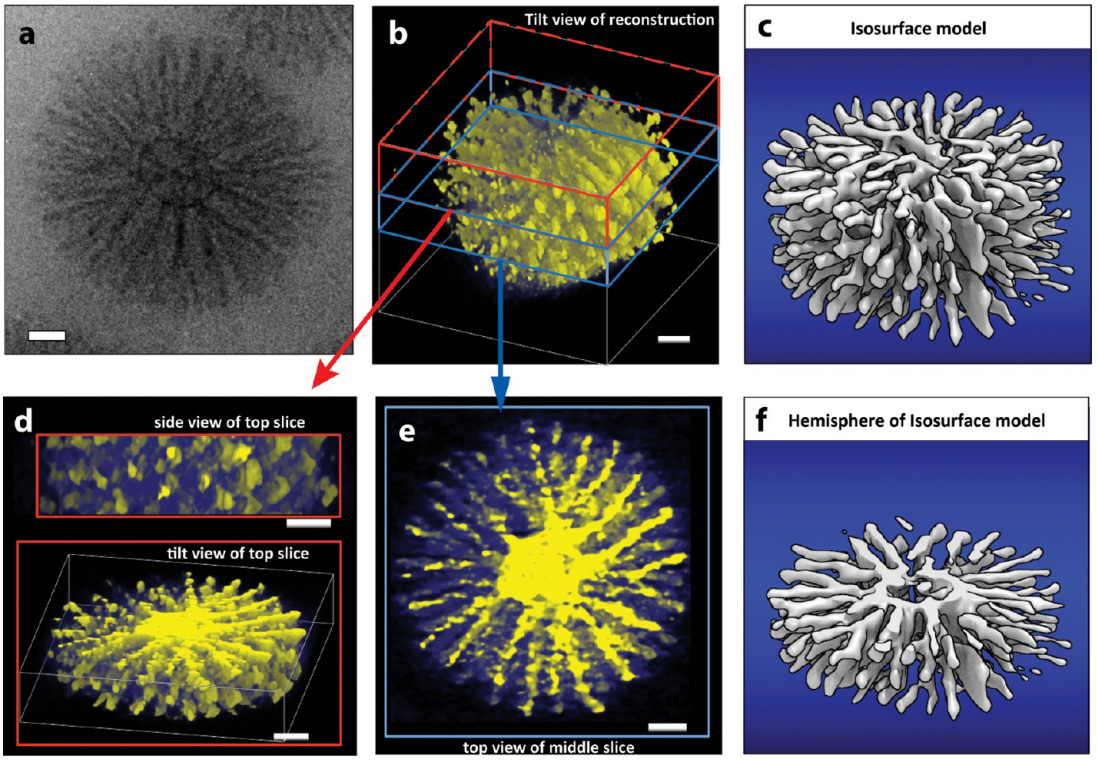

Figure 2. Cryo-ET reconstruction of IPEC1 ($BVqMAA_{1170}/LL_{40}EO_{270}$). (a) Cryo-TEM image of the reconstructed micelles. (b) Overview of reconstruction. The colored frames indicate entire reconstruction (white), top slice (red), and middle slice (blue). (c) Isosurface of entire reconstructed micelle. (d) Side and tilt view of top slice (red). (e) Top view of middle slice (blue). (f) Isosurface of micelle cropped to hemisphere. Scale bars correspond to 50 nm.

core (Figure 2e,f). The overall shape of the otherwise sphere micellar IPEC appears slightly flattened, reminiscent of a bulgy cylinder, which is an effect of sample preparation. The soft particles are deformed by the limited thickness of the solvent film that is close to the diameter of the particle ($\langle D_h \rangle_{z,app} \approx 280$ nm). Nevertheless, the reconstruction unambiguously proves the cylindrical brush morphology of IPEC1. The cylindrical IPEC brushes on a sphere occupy a considerable volume within the confined space of the corona. The hydrophilic PEO chains phase separate and intercalate between the charge-neutral, hydrophobic IPEC domains. The large quantity of polymer chains and the hydrolytic pressure within the water-soluble PEO phase force the corona chains into a stretched conformation.[33] At the same time, the PEO brush provides steric stabilization for the IPEC, which then adapts the cylindrical brush morphology instead of the usually observed collapsed homogeneous shell.[22] The PEO chains not only occupy the space between individual IPEC domains but also form an additional corona surrounding and stabilizing the entire micellar IPECs.

Self-Assembly of IPEC2. For the formation of IPEC2 we chose a diblock copolymer, $Dq_{82}EO_{114}$, where the cationic chain is twice as long as for $LL_{40}EO_{270}$, while the PEO block has less than half the length (Figure 3). According to eq 1, we reach charge neutralization by grafting 14.3 chains of $Dq_{82}EO_{114}$ to each $BVqMAA_{1170}$ chain (ζ-potential ≈ -5 mV). With $N_{agg} \approx 650$, about 9300 chains of $Dq_{82}EO_{114}$ are required for quantitative complexation. From the alternating bright and dark regions found in cryo-TEM (Figure 3), one might assume a similar cylindrical brush morphology to that described above, however with slight differences in appearance. Most notably, the elongated rays of IPEC2 are thicker, more pronounced, and fewer in number as compared to IPEC1. We again assume that PEO chains are located between the IPEC domains as well as expand to the outside of the whole micellar IPEC. However, the zoom-in of Figure 3b,c depicts one IPEC2 particle where continuous stripes are present across the entire core. The pronounced stripes clearly differ from the rays of IPEC1. Blurring of only some corona segments points toward an anisotropic morphology and random orientation of particles toward the observation direction. Throughout the sample we observe partially or entirely blurred particle peripheries at constant viewing angle (Figure S2), further corroborating the assumption of anisotropy.

Cryo-ET Characterization of IPEC2. In the following, we will first elaborate on the larger particle (Figure 3b $d \approx 300$ nm) and classify its morphology, and then proceed to discuss peculiarities regarding the smaller (Figure 3c, $d < 200$ nm) particles. Figure 4 summarizes the cryo-ET of IPEC2, featuring a high IPEC brush

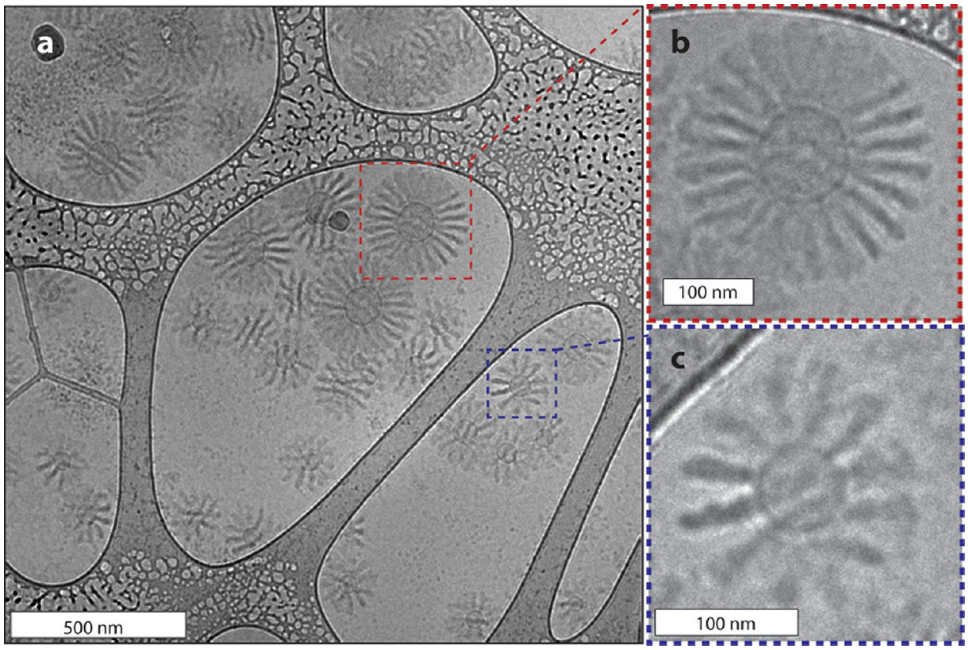

Figure 3. Cryo-TEM of IPEC2 ($BVqMAA_{1170}/Dq_{82}EO_{114}$). (a) Cryo-TEM overview of IPEC2 with striped structural features. (b, c) Zoom-in of selected particles with high (b) and low IPEC brush density.

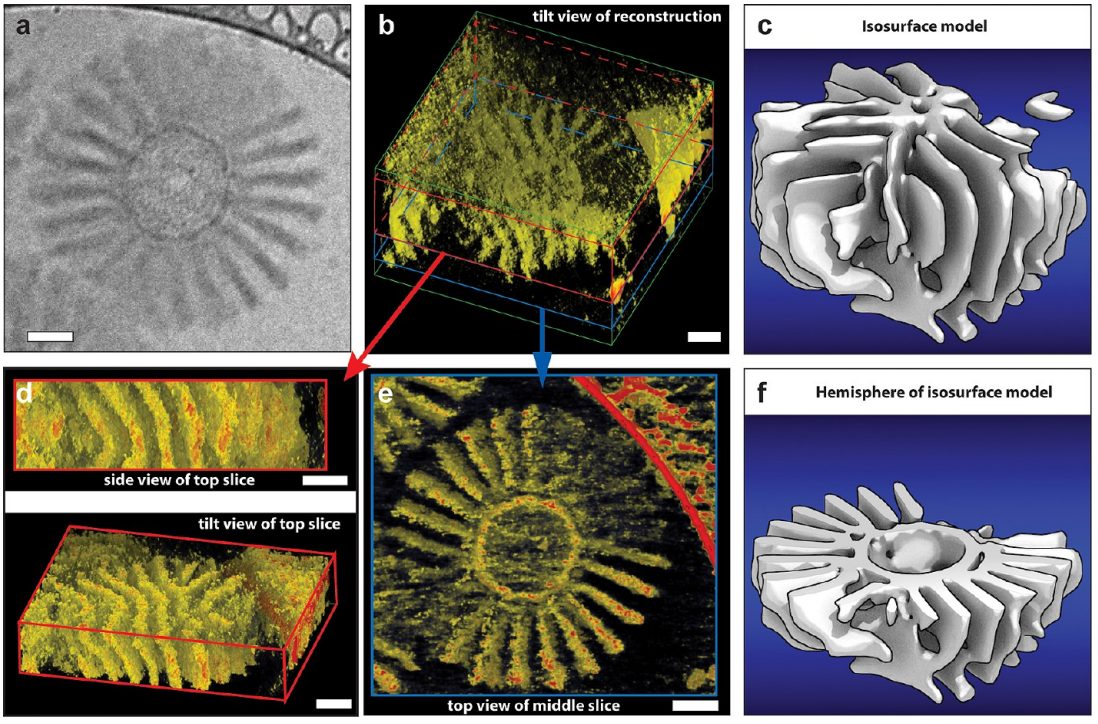

Figure 4. Cryo-ET reconstruction of IPEC2 ($BVqMAA_{1170}/Dq_{82}EO_{114}$). (a) Cryo-TEM image of the reconstructed micelles. (b) Overview of reconstruction. The colored frames indicate entire reconstruction (green), top slice (red), and middle slice (blue). (c) Isosurface of entire reconstructed micelle. (d) Side and tilt view of top slice (red). (e) Top view of middle slice (blue). (f) Isosurface of micelle cropped to hemisphere. Scale bars correspond to 50 nm.

density (see also Supporting Movies SM3 and SM4). Surprisingly, we learn from the 3D reconstruction (Figure 4b–f) that the corona is a rather complex arrangement of lamellae. The reconstructed topographic isosurface of the entire particle suggests that the IPEC lamellae are oriented perpendicular to the curved particle core with an overall appearance of a "turbine" (Figure 4c). Moving along the stack of lamellae (from particle center to poles), the lamellae first run parallel and become progressively more bent when approaching the particle poles (Figure 4d). The cross-section in Figure 4e and the reconstructed isosurface in

Figure 4f show regions of equal electron density (in Figure 4e displayed as yellow = medium and red = high electron contrast). Both the IPEC lamellae and the bumpy *im*-IPEC shell on the particle core have similar contrast, which can be expected since both phases consist of similar polyelectrolytes. Since reconstruction visualizes differences in electron densities and the PB core has a contrast close to that of the background, the isosurface model of Figure 4f exclusively shows the IPECs with a seemingly hollow core. The flattening of the poles is again an effect of the finite thickness of the solvent film that compresses and deforms the particle. The existence of poles might also be an indication for defects that must occur when two immiscible phases (IPEC and PEO) arrange on a spherical substrate (particle core). The lamellae may thus curve to obey defect rules,[55] which could be the explanation why for some particles the lamellar features are well-visible, while they overlap and blur on others (even within the same particle; see also Figure S2).

Figure 5a,b show the cryo-TEM image and the 3D reconstruction of the smaller IPEC2 particles that originate from lower aggregation number. Cryo-ET reveals that on the smaller particle core with high curvature and lower surface area (as compared to larger particles) the lamellae are bent so that they fuse into one continuous spiral from top to bottom of this particle (Figure 5c,d and Supporting Movie SM5). Figure 5c shows the reconstruction as a solid isosurface with the core erased for clarity as to visualize the remaining IPEC2 spiral. The red ribbon is a guide to the eye, which is also displayed as a separate item in Figure 5d. This morphology is surprising given the rigid properties ascribed to polyionic complexes[31] and the seemingly stiff morphologies we discussed so far. We hypothesize that the helical arrangement of the IPEC is actually the favored structure, which we are not able to distinguish for the larger particles due to particle deformation within the solvent film. The smaller particles are located entirely in the vitrified film, allowing visualization of the undisturbed helical conformation of the IPEC2 particles (see also Figure S3 for image series at varying angles).

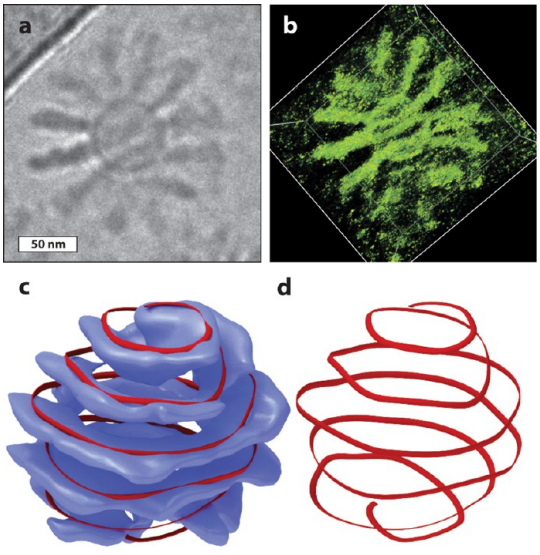

Figure 5. Characterization of the IPEC2 spiral morphology. (a) Cryo-TEM showing a spherical core and IPEC lamellae bent toward the core. (b) Reconstruction of the particle in (a). (c) Core-subtracted isosurface of reconstruction (blue) with a red spiral as a guide to the eye. (d) The red spiral of (c) progressing from top to bottom.

Thermodynamic Stability of IPEC2. To establish whether IPEC2 is the thermodynamically favored morphology or is kinetically trapped by the fast complexation with $Dq_{82}EO_{114}$ (possibly relaxation of IPEC lamellae to cylinders), we followed the development of phase separation into lamellae by studying different $Z_{+/-}$ values and, thus, grafting density (Figure S4). At $Z_{+/-} = 0.25$ (low grafting density), the corona is barely visible as a shadow in cryo-TEM. With increasing $Dq_{82}EO_{114}$ content ($Z_{+/-} = 0.5$), the phase separation of the newly formed hydrophobic IPEC2 from the PEO/water phase becomes more evident in the form of a dark (higher electron density) striped halo surrounding the micellar core. At $Z_{+/-} = 1$, the IPEC nanophase is fully developed and can be distinguished from the PEO/water phase. Following the complexation with DLS, the hydrodynamic radius decreases from $\langle R_h \rangle_{z,app} = 172$ nm for the ($Z_{+/-} = 0$) precursor micelles with a fully stretched PMAA corona to $\langle R_h \rangle_{z,app} = 99$ nm for the contracted, densely grafted IPEC after quantitative complexation with $Dq_{82}EO_{114}$ ($Z_{+/-} = 1$). In order to verify whether the proposed IPEC lamellae are the energetically favored structure, we increased the ionic strength from approximately 50 mM of the original buffer solution to 1000 mM by addition of NaCl (Figure S5). The screening of charges leads to the complete breakup of the IPEC morphology, and although the lamellar features completely vanish, the $Dq_{82}EO_{114}$ chains are assumed to remain entangled within the PMAA corona visible as a homogeneous, fuzzy shell. The added salt enhances chain mobility and causes the order−disorder transition from well-organized packed chains into a diffuse shell. Very similar structures were reported before by Schacher *et al.* complexing shorter corona chains with a longer cationic homopolymer.[21] After reducing the ionic strength by dialysis, the lamellar IPEC morphology is fully restored, indicating that the structure is energetically favored and not kinetically trapped.

Origin of the Structural Differences between IPEC1 and IPEC2. On the basis of the results of cryo-TEM and cryo-ET, we summarize the structural peculiarities of IPECs 1 and 2 in Figure 6 and give schematic suggestions for chain complexation and packing. Figure 6a−d compare both IPEC types with the help of isosurface models and schematic drawings. The isosurface models were calculated from the 3D reconstruction using an algorithmic approach (see Methods and the

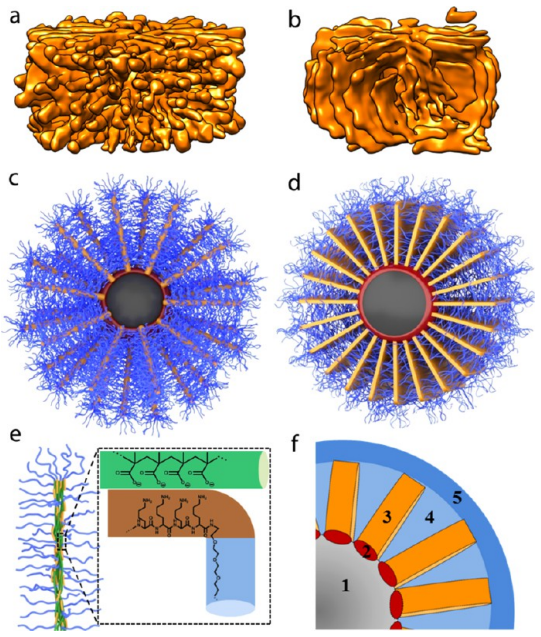

Figure 6. Summary of particle features. (a, b) Isosurface model of the (a) "sea-urchin" micelles and (b) "turbine" micelles. (b, c) Corresponding schematic cross-sectional cartoons. (e, f) Both particle types have the block copolymer chain arrangements (e) in common as well as the distinct order of nanophases (f): (1) PB core, (2) *im*-IPEC, (3) secondary IPEC, (4) intercalated PEO brush, and (5) outer PEO corona.

Supporting Information). From the isosurface models and the schematic drawings one can derive commonalities between both particle types regarding the chain arrangement within the IPEC and the resulting nanophases (Figure 6e–f). Clearly, the dimensions of the IPECs are very different in both cases. The IPEC1 cylinders are longer and thinner compared to the IPEC2 lamellae. In general, the width of the cylinders or lamellae is too large for one single PMAA/polycation chain, but suggests that several ionically grafted chains bundle together (Figure 6e). To compensate the electrostatic repulsion among multiple PMMA chains, the polycations must protrude into the corona bundles and interdigitate with the polyanionic chains to reach charge neutrality. This observation is directly related to the block length of the polycations used for complexation reactions. For IPEC1 a shorter polycationic block is used, which is unable to penetrate as deep into the polyanion bundle as the longer polycationic block for the formation of the IPEC2 particles.

To understand the formation of cylinders and lamellae, we determine the volume fractions of collapsed, hydrophobic IPEC domains, ϕ_{IPEC}, from the isosurface reconstructions (see the Supporting Information for calculations). We obtain a volume fraction of $\phi_{IPEC1} \approx 0.21$ for IPEC1 and $\phi_{IPEC2} \approx 0.43$ for IPEC2 (Figures S6 and S7), which are close to typical values for cylinder and lamellar bulk morphologies for highly incompatible blocks. This supports our hypothesis that the observed brush morphologies indeed originate from the occupied volumes of IPEC and PEO domains. Irrespective of the geometry of the IPEC, we classify five distinct nanodomains for all particles (Figure 6f): (1) the central hydrophobic PB core; (2) a patchy intramicellar IPEC shell surrounding the core; (3) the secondary IPEC brush (cylinder or lamellae) growing perpendicular from the core; (4) a PEO brush located between the hydrophobic IPEC domains; and (5) an outer PEO corona surrounding the entire particle.

CONCLUSIONS

We demonstrated the phase separation of organic nanoparticle coronas through interpolyelectrolyte complexation into anisotropic cylindrical and lamellar brush morphologies stabilized by a newly formed PEO corona. Mismatches in chain length of the participating polyions cause dense packing and overcrowding within the nanoparticle corona. This is accompanied by an immense volume requirement of the water-swollen nonionic block that provides steric stabilization for the IPEC and drives segregation into anisotropic geometries. Although the studied particles appear similar in cryo-TEM imaging, cryo-ET and computer-aided 3D reconstruction of the particles allowed identifying cylindrical and lamellar IPEC morphologies, depending on the length of the polycation block of the bishydrophilic diblock copolymer used for the complexation. The volume fraction of the hydrophobic IPEC over the solvent-swollen PEO corona thereby governs the resulting morphology. Strikingly, both IPEC structures are oriented perpendicular to the surface of the particle core. With the aid of cryo-ET we identify a spiral-on-sphere morphology where the IPEC lamellae fuse into a continuous spiral on the spherical core. Smaller particles are vitrified with an undisturbed corona morphology, indicating that the helical arrangement is the favored arrangement of the lamellar IPEC brush. The ability to dissect complex nanostructures into single structural components is a necessary advancement for future characterization of complex soft matter.

METHODS

Materials. *N*,*N*′-Dicyclohexylcarbodiimide (DCC, 99%, Fluka), 4-dimethylaminopyridine (DMAP, 99%, Acros), 1,1,4,7,10,10-hexamethyltriethylenetetramine (HMTETA, 97% Aldrich), copper(I) chloride (CuCl, 99.9% Acros), and pH 10 buffer solution (Titrinorm, VWR International) were used as received. Prior to use, 2-(dimethylamino)ethyl methacrylate (DMAEMA, 98% Aldrich) was passed through a neutral silica column to remove stabilizer. Dioxane, dichloromethane, and acetone were of analytical grade and used as received. α-Methoxy-ω-amino-PEG (PEG-NH2, M_n = 12 000 g/mol, PDI = 1.03) was purchased from NOF Corporation (Tokyo, Japan), and monomethoxy-PEG

(PEG-OH, M_n = 5000 g/mol, PDI = 1.02) was purchased from Aldrich. Concentrated hydrochloric acid (37%) was used as received. Quaternization reactions were performed with either methyl iodide (99%, Merck) in the case of PEO-*b*-PDMAEMA or dimethyl sulfate (Me_2SO_4, >99%, Aldrich) for BVT. Milli-Q water purified with a Millipore filtering system was used in all cases. For dialysis, membranes of regenerated cellulose (Spectrum Laboratories, Spectra/Por MWCO = 3.5 kDa and 12−14 kDa) were used.

Synthesis of $B_{830}V_{180}T_{1350}$ Triblock Terpolymer and Conversion to $B_{830}Vq_{180}MAA_{1350}$. The BVT triblock terpolymer was synthesized *via* sequential living anionic polymerization as reported elsewhere.[56] The polymer was characterized by a combination of MALDI-ToF-MS (molecular weight of PB), ^{1}H NMR (for the composition of $B_{830}V_{180}T_{1350}$), and size exclusion chromatography for the PDI (1.08). The conversion of BVT to BVqMAA micellar solutions was reported in a previous publication.[23]

Synthesis of PEO_{114} Macroinitiator. The PEO_{114}−Br macroinitiator was synthesized *via* Steglich esterification. To a 100 mL three-neck round-bottom flask equipped with a magnetic stirrer 5.0 g (1.00 mmol) of monomethoxypoly(ethylene glycol) (M_n = 5000, PDI = 1.02), a catalytic amount of DMAP (24.4 mg, 0.02 mmol), and 1.03 g (5 mmol) of DCC were added, and all reactants were dissolved in 30 mL of dry DCM. The mixture was stirred at RT until complete dissolution of PEO. This solution was put in an ice bath, and 0.47 g (3.00 mmol) of 2-bromoisobutyric acid dissolved in 5 mL of dichloromethane was added dropwise under a nitrogen atmosphere. The reaction solution was stirred at room temperature for 18 h, and produced salt was filtered. DCM was removed with a rotary evaporator. The white residue was dissolved in 40 mL of ethanol by heating (50 °C). The clear yellowish solution then was rapidly cooled with liquid nitrogen, and recrystallized PEO_{114}-Br centrifuged in order to remove the soluble compounds by decantation while the product remained precipitated. This procedure was repeated several times until the solution became clear and colorless. Finally the product was dissolved in dioxane and freeze-dried overnight. In this manner 4.10 g of white powder could be obtained, corresponding to a yield of 95%.

Synthesis of PEO_{114}-*b*-$PDMAEMA_{82}$ Diblock Copolymer. The PEO-*b*-PDMAEMA diblock copolymer was synthesized by ATRP in acetone. The PEO macroinitiator with M_n = 5000 g/mol (3.00 g, 1.5 mmol), CuCl (0.15 g, 1.5 mmol), DMAEMA (17.67 g, 113.0 mmol), and 40 mL of acetone were added to a 100 mL screw cap glass equipped with a magnetic stir bar. In another 10 mL screw cap glass the ligand (HMTETA, 0.81 g, 3.0 mmol) was dissolved in 2 mL of acetone (plus 5 ml acetone as excess for degassing). Both solutions were purged with nitrogen separately for about 20 min to remove traces of oxygen. The ligand then was transferred to the 100 mL screw cap glass with a nitrogen-flushed syringe, and the solution was immersed in a thermostated oil bath at 50 °C. The reaction was continued under stirring for 2 h and quenched by cooling to room temperature und exposure to air. In order to remove the catalyst, the solution was diluted with THF and passed through a neutral silica column. The eluent was concentrated using a rotary evaporator. The highly viscous PEO-*b*-PDMAEMA was dissolved in a small amount of THF and precipitated in cold *n*-hexane (−30 °C) followed by freeze-drying from water. From SEC measurements a PDI of 1.17 was obtained, using PEO standards for calibration and from ^{1}H NMR measurement a composition of PEO_{114}-*b*-$PDMAEMA_{82}$ was determined.

Quaternization of PEO-*b*-PDMAEMA. The quaternization of the PEO-*b*-PDMAEMA block copolymer was performed with methyl iodide in aqueous solution. In a typical experiment, 100 mg of the PEO-*b*-PDMAEMA diblock copolymer was dissolved in 10 mL of deionized water. Then, 10 equivalents of methyl iodide (compared to DMAEMA units) was added to the solution while stirring. After 2 days, the polymer solution was dialyzed against dioxane/water (50:50 v/v) and then THF to remove excess methyl iodide and finally back to Milli-Q water. The resulting PEO-*b*-PDMAEMAq ($Dq_{82}EO_{114}$) was recovered as a powder by freeze-drying.

Synthesis of PEO_{270}-*b*-PLL_{40} Diblock Copolymer. The synthesis of the PEO-*b*-PLL diblock copolymer was described in detail in a previous publication.[32] In short, the *N*-carboxy anhydride of the trifluoroacetyl protected L-lysine was first dissolved in dry DMF under an argon atmosphere. Afterward, α-methoxy-ω-amino PEG dissolved in DMF was added to the protected L-lysine, and the mixture was stirred at 25 °C for 72 h until the polymerization was completed. After dialysis against methanol and freeze-drying from dioxane, the PLL block was deprotected under basic conditions (NaOH containing MeOH) by stirring for 10 h at 35 °C. Purification was performed by dialysis against a pH 4 aqueous solution with subsequent freeze-drying. A PDI of 1.05 of the protected diblock copolymer was measured with SEC using DMF as eluent, using PEO standards for calibration. From ^{1}H NMR measurement a composition of PEO_{270}-*b*-PLL_{40} was determined.

Preparation of IPEC1 Solutions. For complexation reactions of IPEC1, the precursor micelles were first transferred to a PBS buffer solution (pH 7.4 with additional 140 mM NaCl). After addition of a certain amount of a 10 g/L stock solution of $LL_{40}EO_{270}$ in PBS, the mixture was stirred for at least 7 days. Additionally cross-linking with *N*-(3-(dimethylamino)propyl)-*N*′-ethylcarbodiimide hydrochloride was performed according to a recipe described elsewhere.[32]

Preparation of IPEC2 Solutions. $Dq_{82}EO_{114}$ was first dissolved in pH 10 buffer to give a 5 g/L solution. Afterward, a defined amount of the $Dq_{82}EO_{114}$ solution was added to 2 mL of a 0.56 g/L solution of BVqMAA precursor micelles in pH 10 buffer solution while stirring to reach full complexation and a $Z_{+/-}$-value of 1. The IPEC solution was stirred for a week at room temperature before analysis.

Characterization. *^{1}H NMR.* Spectra were recorded on a Bruker Ultrashield 300 spectrometer with a 300 MHz operating frequency using either deuterated chloroform or deuterated water as solvents.

Size Exclusion Chromatography (SEC). Size exclusion chromatography measurements were performed on a set of 30 cm SDV-gel columns of 5 mm particle size having a pore size of 10^5, 10^4, 10^3, and 10^2 Å with refractive index and UV (λ = 254 nm) detection. SEC was measured at an elution rate of 1 mL/min with THF as eluent. For $LL_{40}EO_{270}$ a Tosoh instrument (Yamaguchi, Japan) calibrated with PEG standards and equipped with three TSK columns (TSK guard column HHR-L; TSKgel G4000HHR; TSKgel G3000HHR) and a refractive index detector (RI) at 40 °C was used. DMF with 10 mM LiCl was used as eluent at a flow rate of 0.8 mL/min.

Dynamic Light Scattering. Measurements were performed on an ALV DLS/SLS-SP 5022F compact goniometer system with an ALV 5000/E cross correlator and a He−Ne laser (λ = 632.8 nm). The measurements were carried out in cylindrical scattering cells (d = 10 mm) at an angle of 90°. Prior to the measurements samples were passed through nylon filters (Magna, Roth) with a pore size of 5 μm to remove impurities/dust particles. The CONTIN algorithm was applied to analyze the obtained correlation functions. Apparent hydrodynamic radii ($\langle R_h \rangle_{z,app}$) were calculated according to the Stokes−Einstein equation, and polydispersities were obtained *via* the cumulant analysis where applicable.

ζ-Potential Measurements. Measurements were performed with disposable capillary cells (DTS1061) on a Malvern Zetasizer, using approximately 800 μL of the aqueous micellar solutions. The ζ-potential was calculated from electrophoretic mobility applying the Smoluchowski equation.

Cryogenic Transmission Electron Microscopy. Cryo-TEM measurements were performed at the University of Bayreuth as well as at Aalto University. For cryo-TEM studies at the University of Bayreuth, 3 μL of the aqueous micellar solution ($c \approx 0.5$ g/L) was placed on a lacey carbon-coated copper TEM grid (200 mesh, Science Services), where most of the liquid was blotted with filter paper, leaving a thin film spread between the fibers of the carbon network. The specimens were shock vitrified by rapid immersion into liquid ethane in a temperature-controlled freezing unit (Zeiss Cryobox, Zeiss NTS GmbH) and cooled to approximately −183°C. The temperature was monitored and kept constant in the chamber during all of the preparation steps. After freezing the specimens they were inserted into a cryo-transfer holder (CT3500, Gatan) and transferred to a Zeiss EM922 Omega EFTEM instrument. Measurements were carried out at temperatures around −183°C. The microscope was operated at an acceleration voltage of 200 kV. Zero-loss filtered images (ΔE = 0 eV) were taken under reduced dose conditions. All images were

recorded digitally by a bottom-mounted CCD camera system (Ultrascan 1000, Gatan) and processed with a digital imaging processing system (Gatan Digital Micrograph 3.9 for GMS 1.4). For cryo-TEM measurements at Aalto University, imaging was carried out using a JEM 3200FSC field emission microscope (Jeol) operated at 300 kV in bright field mode with an Omega-type zero-loss energy filter. The images were acquired with an Ultrascan 4000 CCD camera (Gatan) and with Gatan Digital Micrograph software (version 1.83.842), while the specimen temperature was maintained at −187 °C. Vitrified samples were prepared using a FEI Vitribot placing 3 μL of sample solution on 200-mesh holey carbon copper grids under 100% humidity, then blotted with filter paper for 0.5−1.5 s, and immediately plunged into a −170 °C ethane/propane mixture and cryotransfered to the microscope.

Cryogenic Transmission Electron Tomography. Cryo-ET measurements were performed at Aalto University with the same transmission electron microscope that was used for cryo-TEM imaging. Electron tomographic tilt series were acquired with the SerialEM software package (version 3.2.2). Samples were tilted between ±69° angles with 2−3° increment steps. For a detailed description of the alignment and reconstruction procedure see the Supporting Information.

Conflict of Interest: The authors declare no competing financial interest.

Supporting Information Available: Figures S1−S7, Tables S1, supporting calculations, descriptions of the cryo-ET method, and Supporting Movies SM1−SM5. This material is available free of charge *via* the Internet at http://pubs.acs.org.

Acknowledgment. The authors acknowledge the Deutsche Forschungsgemeinschaft (DFG) for supporting this work within DFG Mu896/39-1. This work was carried out under the Academy of Finland's Centre of Excellence Programme (2014−2019) and supported by ERC-2011-AdG (291364-MIMEFUN). This work made use of the Aalto University Nanomicroscopy Center (Aalto-NMC) premises.

REFERENCES AND NOTES

1. Glotzer, S. C.; Solomon, M. J. Anisotropy of Building Blocks and Their Assembly into Complex Structures. *Nat. Mater.* **2007**, *6*, 557–562.
2. Walther, A.; Müller, A. H. E. Janus Particles: Synthesis, Self-Assembly, Physical Properties, and Applications. *Chem. Rev.* **2013**, *113*, 5194–5261.
3. Du, J.; O'Reilly, R. K. Anisotropic Particles with Patchy, Multicompartment and Janus Architectures: Preparation and Application. *Chem. Soc. Rev.* **2011**, *40*, 2402–2416.
4. Zhu, J.; Zhang, S.; Zhang, K.; Wang, X.; Mays, J. W.; Wooley, K. L.; Pochan, D. J. Disk-Cylinder and Disk-Sphere Nanoparticles via a Block Copolymer Blend Solution Construction. *Nat. Commun.* **2013**, *4*, 2297.
5. Rupar, P. A.; Chabanne, L.; Winnik, M. A.; Manners, I. Non-Centrosymmetric Cylindrical Micelles by Unidirectional Growth. *Science* **2012**, *337*, 559–562.
6. Gröschel, A. H.; Schacher, F. H.; Schmalz, H.; Borisov, O. V.; Zhulina, E. B.; Walther, A.; Müller, A. H. E. Precise Hierarchical Self-Assembly of Multicompartment Micelles. *Nat. Commun.* **2012**, *3*, 710.
7. Moughton, A. O.; Hillmyer, M. A.; Lodge, T. P. Multicompartment Block Polymer Micelles. *Macromolecules* **2012**, *45*, 2–19.
8. Bates, F. S.; Hillmyer, M. A.; Lodge, T. P.; Bates, C. M.; Delaney, K. T.; Fredrickson, G. H. Multiblock Polymers: Panacea or Pandora's Box? *Science* **2012**, *336*, 434–440.
9. Wyman, I. W.; Liu, G. Micellar Structures of Linear Triblock Terpolymers: Three Blocks but Many Possibilities. *Polymer* **2013**, *54*, 1950–1978.
10. Zhang, L.; Yu, K.; Eisenberg, A. Ion-Induced Morphological Changes in "Crew-Cut" Aggregates of Amphiphilic Block Copolymers. *Science* **1996**, *272*, 1777–1779.
11. Förster, S.; Hermsdorf, N.; Böttcher, C.; Lindner, P. Structure of Polyelectrolyte Block Copolymer Micelles. *Macromolecules* **2002**, *35*, 4096–4105.
12. Pergushov, D. V.; Müller, A. H. E.; Schacher, F. H. Micellar Interpolyelectrolyte Complexes. *Chem. Soc. Rev.* **2012**, *41*, 6888–6901.
13. Sharma, G.; Mei, Y.; Lu, Y.; Ballauff, M.; Irrgang, T.; Proch, S.; Kempe, R. Spherical Polyelectrolyte Brushes as Carriers for Platinum Nanoparticles in Heterogeneous Hydrogenation Reactions. *J. Catal.* **2007**, *246*, 10–14.
14. Wittemann, A.; Haupt, B.; Ballauff, M. Adsorption of Proteins on Spherical Polyelectrolyte Brushes in Aqueous Solution. *Phys. Chem. Chem. Phys.* **2003**, *5*, 1671–1677.
15. Wittemann, A.; Ballauff, M. Interaction of Proteins with Linear Polyelectrolytes and Spherical Polyelectrolyte Brushes in Aqueous Solution. *Phys. Chem. Chem. Phys.* **2006**, *8*, 5269–5275.
16. Wang, S.; Chen, K.; Li, L.; Guo, X. Binding between Proteins and Cationic Spherical Polyelectrolyte Brushes: Effect of pH, Ionic Strength, and Stoichiometry. *Biomacromolecules* **2013**, *14*, 818–827.
17. Haupt, B.; Neumann, T.; Wittemann, A.; Ballauff, M. Activity of Enzymes Immobilized in Colloidal Spherical Polyelectrolyte Brushes. *Biomacromolecules* **2005**, *6*, 948–955.
18. Harada, A.; Kataoka, K. Chain Length Recognition: Core-Shell Supramolecular Assembly from Oppositely Charged Block Copolymers. *Science* **1999**, *283*, 65–67.
19. Gohy, J.-F.; Varshney, S. K.; Jérôme, R. Water-Soluble Complexes Formed by Poly(2-vinylpyridinium)-block-Poly(ethylene oxide) and Poly(sodium methacrylate)-block-Poly(ethylene oxide) Copolymers. *Macromolecules* **2001**, *34*, 3361–3366.
20. Schacher, F.; Walther, A.; Müller, A. H. E. Dynamic Multicompartment-Core Micelles in Aqueous Media. *Langmuir* **2009**, *25*, 10962–10969.
21. Schacher, F.; Betthausen, E.; Walther, A.; Schmalz, H.; Pergushov, D. V.; Müller, A. H. E. Interpolyelectrolyte Complexes of Dynamic Multicompartment Micelles. *ACS Nano* **2009**, *3*, 2095–2102.
22. Synatschke, C. V.; Schacher, F. H.; Förtsch, M.; Drechsler, M.; Müller, A. H. E. Double-Layered Micellar Interpolyelectrolyte Complexes—How Many Shells to a Core? *Soft Matter* **2011**, *7*, 1714–1725.
23. Synatschke, C. V.; Löbling, T. I.; Förtsch, M.; Hanisch, A.; Schacher, F. H.; Müller, A. H. E. Micellar Interpolyelectrolyte Complexes with a Compartmentalized Shell. *Macromolecules* **2013**, *46*, 6466–6474.
24. Kabanov, V. A. Polyelectrolyte Complexes in Solution and in Bulk. *Russ. Chem. Rev.* **2005**, *74*, 3–20.
25. Lefèvre, N.; Fustin, C.-A.; Gohy, J.-F. Polymeric Micelles Induced by Interpolymer Complexation. *Macromol. Rapid Commun.* **2009**, *30*, 1871–1888.
26. Pergushov, D. V.; Zezin, A. A.; Zezin, A. B.; Müller, A. H. E. Advanced Functional Structures Based on Interpolyelectrolyte Complexes. *Adv. Polym. Sci.* **2014**, *255*, 173–225.
27. Schrage, S.; Sigel, R.; Schlaad, H. Formation of Amphiphilic Polyion Complex Vesicles from Mixtures of Oppositely Charged Block Ionomers. *Macromolecules* **2003**, *36*, 2–5.
28. Plamper, F. A.; Gelissen, A. P.; Timper, J.; Wolf, A.; Zezin, A. B.; Richtering, W.; Tenhu, H.; Simon, U.; Mayer, J.; Borisov, O. V.; *et al.* Spontaneous Assembly of Miktoarm Stars into Vesicular Interpolyelectrolyte Complexes. *Macromol. Rapid Commun.* **2013**, *34*, 855–860.
29. Anraku, Y.; Kishimura, A.; Oba, M.; Yamasaki, Y.; Kataoka, K. Spontaneous Formation of Nanosized Unilamellar Polyion Complex Vesicles with Tunable Size and Properties. *J. Am. Chem. Soc.* **2010**, *132*, 1631–1636.
30. Voets, I. K.; Keizer, A.; De Waard, P.; De Frederik, P. M.; Bomans, P. H. H.; Schmalz, H.; Walther, A.; King, S. M.; Leermakers, F. A. M.; Stuart, M. A. C. Double-Faced Micelles from Water-Soluble Polymers. *Angew. Chem., Int. Ed.* **2006**, 6673–6676.
31. Christian, D. A.; Tian, A.; Ellenbroek, W. G.; Levental, I.; Rajagopal, K.; Janmey, P. A.; Liu, A. J.; Baumgart, T.; Discher, D. E. Spotted Vesicles, Striped Micelles and Janus Assemblies Induced by Ligand Binding. *Nat. Mater.* **2009**, *8*, 843–849.
32. Synatschke, C. V.; Nomoto, T.; Cabral, H.; Förtsch, M.; Toh, K.; Matsumoto, Y.; Miyazaki, K.; Hanisch, A.; Schacher, F. H.;

Kishimura, A.; *et al.* Multicompartment Micelles with Adjustable Poly(ethylene Glycol) Shell for Efficient in Vivo Photodynamic Therapy. *ACS Nano* **2014**, *8*, 1161–1172.
33. Larin, S. V.; Pergushov, D. V.; Xu, Y.; Darinskii, A. A.; Zezin, A. B.; Müller, A. H. E.; Borisov, O. V. Nano-Patterned Structures in Cylindrical Polyelectrolyte Brushes Assembled with Oppositely Charged Polyions. *Soft Matter* **2009**, *5*, 4938–4943.
34. Pons-Siepermann, I. C.; Glotzer, S. C. Design of Patchy Particles Using Quaternary Self-Assembled Monolayers. *ACS Nano* **2012**, *6*, 3919–3924.
35. Kostiainen, M. A.; Hiekkataipale, P.; Laiho, A.; Lemieux, V.; Seitsonen, J.; Ruokolainen, J.; Ceci, P. Electrostatic Assembly of Binary Nanoparticle Superlattices Using Protein Cages. *Nat. Nanotechnol.* **2013**, *8*, 52–56.
36. Chen, Q.; Diesel, E.; Whitmer, J. K.; Bae, S. C.; Luijten, E.; Granick, S. Triblock Colloids for Directed Self-Assembly. *J. Am. Chem. Soc.* **2011**, *133*, 7725–7727.
37. Chen, Q.; Bae, S. C.; Granick, S. Staged Self-Assembly of Colloidal Metastructures. *J. Am. Chem. Soc.* **2012**, *134*, 11080–11083.
38. Gröschel, A. H.; Walther, A.; Löbling, T. I.; Schmelz, J.; Hanisch, A.; Schmalz, H.; Müller, A. H. E. Facile, Solution-Based Synthesis of Soft, Nanoscale Janus Particles with Tunable Janus Balance. *J. Am. Chem. Soc.* **2012**, *134*, 13850–13860.
39. Wang, X.; Guerin, G.; Wang, H.; Wang, Y.; Manners, I.; Winnik, M. A. Cylindrical Block Copolymer Micelles and Co-Micelles of Controlled Length and Architecture. *Science* **2007**, *317*, 644–647.
40. Hudson, Z. M.; Lunn, D. J.; Winnik, M. A.; Manners, I. Colour-Tunable Fluorescent Multiblock Micelles. *Nat. Commun.* **2014**, *5*, 3372.
41. Schmelz, J.; Karg, M.; Hellweg, T.; Schmalz, H. General Pathway toward Crystalline-Core Micelles with Tunable Morphology and Corona Segregation. *ACS Nano* **2011**, *5*, 9523–9534.
42. Zhong, S.; Pochan, D. J. Cryogenic Transmission Electron Microscopy for Direct Observation of Polymer and Small-Molecule Materials and Structures in Solution. *Polym. Rev.* **2010**, *50*, 287–320.
43. Newcomb, C. J.; Moyer, T. J.; Lee, S. S.; Stupp, S. I. Advances in Cryogenic Transmission Electron Microscopy for the Characterization of Dynamic Self-Assembling Nanostructures. *Curr. Opin. Colloid Interface Sci.* **2012**, *17*, 350–359.
44. Nudelman, F.; With, G.; de Sommerdijk, N. A. J. M. Cryo-Electron Tomography: 3-Dimensional Imaging of Soft Matter. *Soft Matter* **2011**, *7*, 17–24.
45. Song, F.; Chen, P.; Sun, D.; Wang, M.; Dong, L.; Liang, D.; Xu, R.-M.; Zhu, P.; Li, G. Cryo-EM Study of the Chromatin Fiber Reveals a Double Helix Twisted by Tetranucleosomal Units. *Science* **2014**, *344*, 376–380.
46. Majoinen, J.; Haataja, J. S.; Appelhans, D.; Lederer, A.; Olszewska, A.; Seitsonen, J.; Aseyev, V.; Kontturi, E.; Rosilo, H.; Österberg, M.; *et al.* Supracolloidal Multivalent Interactions and Wrapping of Dendronized Glycopolymers on Native Cellulose Nanocrystals. *J. Am. Chem. Soc.* **2014**, *136*, 866–869.
47. Nudelman, F.; Pieterse, K.; George, A.; Bomans, P. H. H.; Friedrich, H.; Brylka, L. J.; Hilbers, P. A. J.; With, G.; de Sommerdijk, N. A. J. M. The Role of Collagen in Bone Apatite Formation in the Presence of Hydroxyapatite Nucleation Inhibitors. *Nat. Mater.* **2010**, *9*, 1004–1009.
48. McKenzie, B. E.; Nudelman, F.; Bomans, P. H. H.; Holder, S. J.; Sommerdijk, N. A. J. M. Temperature-Responsive Nanospheres with Bicontinuous Internal Structures from a Semicrystalline Amphiphilic Block Copolymer. *J. Am. Chem. Soc.* **2010**, *132*, 10256–10259.
49. Parry, A. L.; Bomans, P. H. H.; Holder, S. J.; Sommerdijk, N. A. J. M.; Biagini, S. C. G. Cryo Electron Tomography Reveals Confined Complex Morphologies of Tripeptide-Containing Amphiphilic Double-Comb Diblock Copolymers. *Angew. Chem., Int. Ed.* **2008**, *47*, 8859–8862.
50. Hanisch, A.; Förtsch, M.; Drechsler, M.; Jinnai, H.; Ruhland, T. M.; Schacher, F. H.; Müller, A. H. E. Counterion-Mediated Hierarchical Self-Assembly of an ABC Miktoarm Star Terpolymer. *ACS Nano* **2013**, *7*, 4030–4041.
51. Dupont, J.; Liu, G.; Niihara, K.; Kimoto, R.; Jinnai, H. Self-Assembled ABC Triblock Copolymer Double and Triple Helices. *Angew. Chem., Int. Ed.* **2009**, *48*, 6144–6147.
52. Hickey, R. J.; Koski, J.; Meng, X.; Riggleman, R. A.; Zhang, P.; Park, S.-J. Size-Controlled Self-Assembly of Superparamagnetic Polymersomes. *ACS Nano* **2014**, *8*, 495–502.
53. Jinnai, H.; Spontak, R. J.; Nishi, T. Transmission Electron Microtomography and Polymer Nanostructures. *Macromolecules* **2010**, *43*, 1675–1688.
54. Hermans, T. M.; Broeren, M. A. C.; Gomopoulos, N.; Schoot, P.; van der Genderen, M. H. P.; van Sommerdijk, N. A. J. M.; Fytas, G.; Meijer, E. W. Self-Assembly of Soft Nanoparticles with Tunable Patchiness. *Nat. Nanotechnol.* **2009**, *4*, 721–726.
55. Zhang, L.; Wang, L.; Lin, J. Defect Structures and Ordering Behaviours of Diblock Copolymers Self-Assembling on Spherical Substrates. *Soft Matter* **2014**, *10*, 6713–6721.
56. Schacher, F.; Yuan, J.; Schoberth, H. G.; Müller, A. H. E. Synthesis, Characterization, and Bulk Crosslinking of Polybutadiene-block-Poly(2-vinyl pyridine)-block-Poly(tert-butyl methacrylate) Block Terpolymers. *Polymer* **2010**, *51*, 2021–2032.